



## SOLIDIFICATION BEHAVIOR IN THE PRESENCE OF EXTERNAL FIELDS

# Effect of Electromagnetic Stirring on the Solidification Behavior of High-Magnetic-Induction Grain-Oriented Silicon Steel Continuous Casting Slab

XIN LI,<sup>1</sup> XIANHUI WANG,<sup>2</sup> YANPING BAO,<sup>1</sup> JIAN GONG,<sup>2</sup>  
WEIGUANG PANG,<sup>2</sup> and MIN WANG<sup>1,3</sup>

1.—State Key Lab of Advanced Metallurgy, University of Science and Technology Beijing, Beijing 100083, China. 2.—Silicon Steel Department, Shougang Qian'an Iron and Steel Company, Qian'an 064404, Hebei, China. 3.—e-mail: wm1013@163.com

The solidification behaviors of high-magnetic-induction grain-oriented silicon steel slabs have been investigated during experiments in industrial strand electromagnetic stirring (S-EMS). The current intensities of S-EMS were 0, 120, 200, and 350 A, and the frequency was 5 Hz. The ratio of the equiaxed crystal was 14.95%, 15.64%, 45.22%, and 66.96%, respectively. Central porosity cannot be eliminated by increasing the current intensity. The number, size, and ratio of segregation spots were markedly reduced by minimizing the equiaxed crystal zone. Carbon in the 0 and 120 A slabs exhibited a lower degree of macrosegregation compared with the 200 and 350 A slabs. Controlling the cooling rate and increasing the total reduction are the directions to further improve solidification structures, defects, and carbon segregation.

## INTRODUCTION

High-magnetic-induction grain-oriented silicon steel is widely used in power generation and transmission fields.<sup>1–3</sup> The final magnetic properties of grain-oriented silicon steel are determined by its chemical composition and structures.<sup>4</sup> With an increase in power demand, the requirements for manufacturing grain-oriented silicon steel increase as well, particularly for controlling the chemical composition and homogeneity distribution of final structures. Continuous casting as the initial link of the long and complex heat treatment and rolling process affects the manufacturing process and final product properties directly. The solidification structures of continuous casting slab have a significant effect on the homogeneous distribution of chemical composition and the formation of highly aligned structures. Segregation behavior cannot be completely removed because of the redistribution of the residual solute enriched in the mushy zone during continuous casting. Segregation can be divided by scale into microsegregation, semi-macroscopic segregation, and macrosegregation,<sup>5–7</sup> which are related to the morphology of the solidification structure. The serious segregation and central

cracks induced by the coarse structure appear in the center zone of the slab.<sup>8</sup> Compared with the texture transformation process of coarse and fine structures of samples, the fine structures are easier to transform into Gaussian texture.<sup>9</sup> Coarse structures need to be prevented during grain-oriented silicon steel industrial production.

To control the morphology of the solidification structures and the redistribution of the enriched residual solute, low superheat, soft reduction, and electromagnetic stirring are typically employed during industrial production. The degree of segregation can be reduced by increasing the equiaxed crystal ratio by low superheat casting.<sup>10,11</sup> Soft reduction casting can effectively improve central segregation by changing the morphology of solidification structures.<sup>12–14</sup> The morphology of solidification structures is mainly determined by the temperature gradient in the solidifying front and the number of nuclei. The coarse structure is usually formed under a large temperature gradient and a small number of nuclei. The temperature gradient, number of nuclei, and redistribution of the enriched residual solute can be strongly changed by electromagnetic stirring. Electromagnetic stirring usually helps refine the solidification structures,

increase the equiaxed crystal ratio, eliminate the internal defects, and decrease the formation of segregation bands.<sup>15</sup> The disadvantage of electromagnetic stirring is that it cannot solve the shrinkage problem of the solidification end, but it can be addressed by soft reduction. Electromagnetic stirring and soft reduction are gradually combined to improve the inner cracks, shrinkage volumes, and segregation during continuous casting.<sup>16–18</sup> As the equiaxed zone ratio increased from 19% to 33%, the maximum degree of carbon segregation decreased from 1.13 to 1.05 by applying electromagnetic stirring and soft reduction during casting.<sup>15</sup>

As previously discussed, controlling solidification structures and segregation behavior by using low superheat, soft reduction, and electromagnetic stirring was an effective technique. Although the principles of each method have been understood, the solidification behavior in grain-oriented silicon steel continuously cast slabs is rarely reported. In the current study, grain-oriented silicon steel slabs were produced by soft reduction and strand electromagnetic stirring (S-EMS) at different current intensities. The morphology of the solidification structures and the distribution of chemical compositions were characterized to evaluate the effect of S-EMS on the solidification behavior of slabs. Optimization directions of the grain-oriented silicon steel were suggested during continuous casting.

## METHODS

Slab caster parameters were set as a constant, except for the in-roll type S-EMS, to investigate the solidification structures of grain-oriented silicon steel slabs. The main parameters of the experiments are listed in Table I. Figure 1 presents the schematic diagram of S-EMS and the sample collection. Samples measuring 230 mm × 40 mm × 40 mm were cut from the center of slabs and etched with hydrochloric acid to reveal the morphology of the solidification structures. The equiaxed crystal ratio (ER) was calculated by Eq. (1).

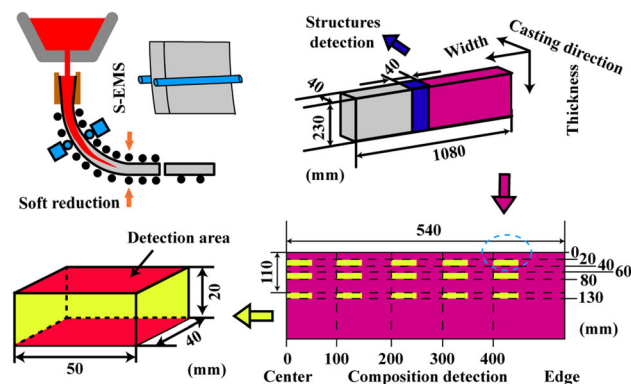


Fig. 1. S-EMS and sample collection.

$$ER = \frac{\text{Average width of the equiaxed crystal zone}}{\text{Average width of the slab}} \times 100\% \quad (1)$$

Samples measuring 50 mm × 40 mm × 20 mm were cut from the slabs to investigate the carbon distribution in the thickness and width directions (Fig. 1). The nominal values of carbon and silicon (wt.%) in the slab are 0.08 and 3.25, respectively. The top and bottom of samples were detected by spark source mass spectrometry (ARL iSpark 8860; diameter of the detection spot, 10 mm) to investigate the carbon concentration (testing value). Four points along the width direction in the 50 mm × 40 mm section were analyzed, and the carbon degree of segregation was calculated using Eq. (2). The total segregation spot area in the center sample was determined by image analysis using the Image-Pro Plus 6.0 image analysis software (Media Cybernetics, Inc., Silver Spring, MD, USA), and the ratio of segregation spots area (RSA) was calculated using Eq. (3).<sup>9</sup>

$$\text{Carbon segregation degree} = \frac{\text{Testing value}}{\text{Nominal value}} \quad (2)$$

Table I. Main parameter of experiments

Item	Value
Slab section size, mm × mm	230 × 1080
Casting speed, m min <sup>-1</sup>	1.2
Soft reduction rate, mm m <sup>-1</sup>	0.15–0.3
Superheat temperature, °C	25–30
Stirring position, mm	6190
Length of S-EMS supporting roller, mm	1700
Strand roller diameter, mm	240
S-EMS coil currents, A	0, 120, 200, 350
Frequency of S-EMS source current, Hz	5

$$\text{RSA}(\%) = \frac{\sum_i^n S_i}{D \times L} \quad (3)$$

where  $D$  and  $L$  refer to the thickness and width of the testing samples.  $S_i$  is the segregation spot area.

## RESULTS AND DISCUSSION

### Morphology of Solidification Structure

Figure 2 illustrates the morphology of the solidification structures under the S-EMS current intensities of 0, 120 A, 200 A, and 350 A. The main structures are the columnar crystal zone (CZ) and the equiaxed crystal zone (EZ), which are separated by the red line in the four slab sections. The columnar-to-equiaxed transition (CET) can be observed clearly in the 200 and 350 A slabs (Fig. 2c, d). For the 0 A, 120 A, 200 A, and 350 A slabs, the ER is 14.95%, 15.64%, 45.22%, and 66.96%, respectively. These results indicate that the ER increases with the current intensity of S-EMS. The asymmetric structures are shown in the 0 A and 120 A slabs (Fig. 2a, b), more symmetrical solidification structures were found in the 200 A and 350 A slabs.

In the present work, the morphology of the solidification structure mainly depends on the cooling conditions and S-EMS. The inner arc surface is a waterlogged surface due to the arc structure of the continuous caster, so the inner arc side cooling rate is greater than the outer arc. Meanwhile, the primary nuclei prefer to deposit in the outer arc side under the influence of gravity, which prevents the development of columnar crystals. The asymmetric and coarse columnar crystal presents in the

inner arc side, and the cooling conditions play the dominant role in 0 A and 120 A slabs. The nuclei prefer to transform into equiaxed crystals under isotropic temperature conditions. The S-EMS improves the fluid flow from the center of the slab to the mushy zone compared with the natural convection, thus decreasing the temperature gradient.<sup>14</sup> Additionally, fast-growing dendrites can be interrupted by the fluid flow powered by S-EMS and soft reduction, further preventing the formation of columnar crystals. The morphology of 200 A and 350 A slabs was dominated by the cooling conditions and S-EMS.

Figure 3 presents the morphology of typical dendrites from the inner surface to the center of slabs, which shows the details of the solidification process. Similar dendrites are observed 20 mm and 50 mm from the inner arc surface of the slabs. The generation direction of dendrites in CET deviates from the solidification direction. There are regularly arranged dendrites in the EZ of 0 A and 120 A slabs. However, the dendrites in the EZ of 200 A and 350 A slabs consist of short and random arrangements. Comparing the solidification structures of 0 A and 120 A slabs, the dendritic arm space and growth direction are hardly changed by the current intensity of 120 A. The stirring efficiency of S-EMS mainly depends on the input current, frequency, and liquid cavity size.<sup>19,20</sup> At the frequency of 5 Hz, the penetration depth of electromagnetic wave in the secondary cooling zone is basically the same. Although the input current increases from 0 A to 120 A, the small electromagnetic force leads to insufficient electromagnetic stirring intensity to effectively change the molten

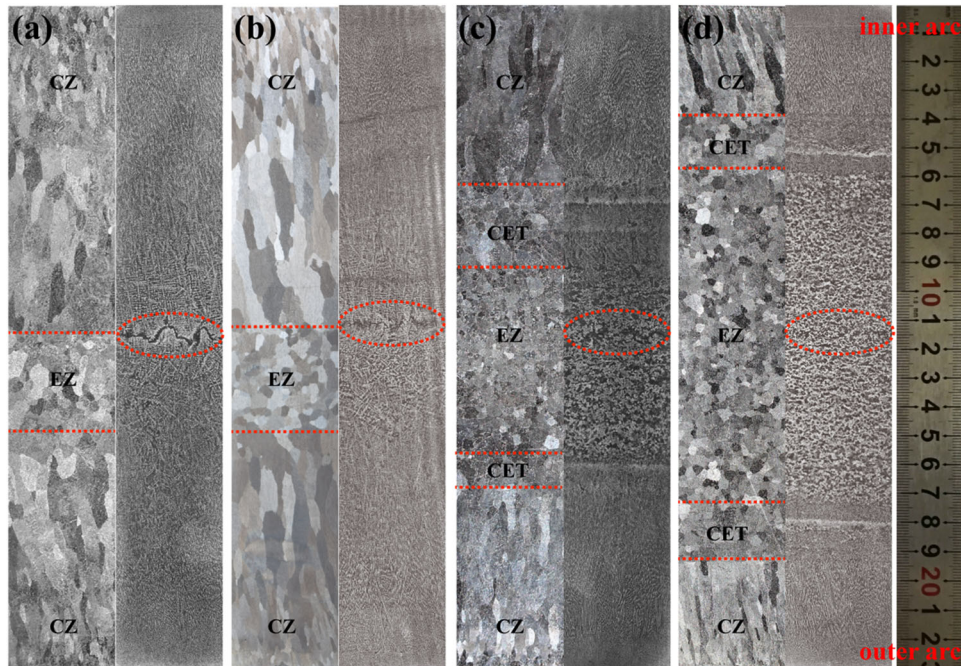


Fig. 2. Solidification structures of slabs under different current intensities: (a) 0, (b) 120, (c) 200, (d) 350 A.



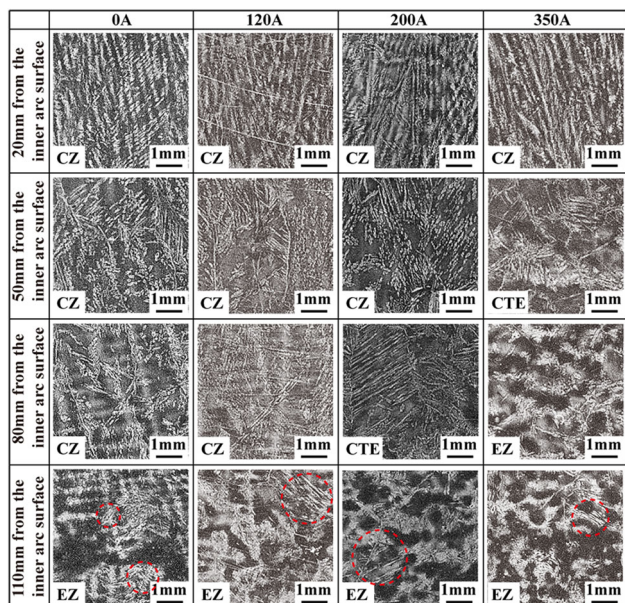


Fig. 3. Morphology of dendritic structure at different positions.

steel flow behavior. To more efficiency stir the molten steel, the electromagnetic force parameter of S-EMS cannot be  $< 120$  A and 5 Hz.

Some fractured dendrites (red circles) smaller than the normal dendrites are found in the EZ of four slabs. Due to the difference in solute distribution around the root of dendrites and the morphology of dendrites, some dendrites can be melted and fractured at the root.<sup>21,22</sup> The S-EMS stirring intensity can be reflected by the deflection and fracture behavior of dendrites. Without considering the solute field, the deflection behavior of dendrites depends on the velocity and temperature field around the dendrites.<sup>23</sup> The superheat at the upstream side of dendrites can be eliminated by fluid flow, which leads to the deflection of dendrites to the upstream side. With the increase of flow rate, the generation direction of dendrites gradually deflects to the flow direction and eventually breaks at the maximum curvature.

Central porosity usually appears at the solidification end, where the molten steel cannot fill the solidification shrinkage spaces.<sup>24,25</sup> Central porosity can be improved by controlling the cooling rate and the soft reduction process. For grain-oriented silicon steel slabs, the central porosity is gradually improved by increasing the current intensity, but it cannot be eliminated. The columnar crystal structures appearing in the 0 A and 120 A slab show that the cooling rate, especially in the inner arc side, is too fast in the present continuous casting. Although the nuclei and residual molten steel are redistributed by S-EMS, many shrinkage spaces remain in the center of the slabs. These results indicate that the soft reduction is not strong enough to eliminate the shrinkage spaces. The optimization directions of central defects decrease

the inner arc side cooling rate and increase the total reduction.

### Solidification Structure and Segregation Spots

Segregation arises from the redistribution of the residual solute-enriched molten steel during solidification. Spot-like spaces usually exist at the interface between dendrites, providing conditions for entrapping solute-enriched molten steel. The size and number of segregation spots significantly depend on the morphology of the solidification structures. Figure 4a presents the statistical results of the number and size of the spots with the section size measuring  $130 \text{ mm} \times 40 \text{ mm}$ . The number of spots is 131 A, 125 A, 546 A, and 664 A in the 0 A, 120 A, 200 A, and 350 A slabs, respectively. The 200 A and 350 A samples have 38 and 46 larger spots (more than  $2 \text{ mm}^2$ ), while the 0 A and 120 A samples have 6 and 4 spots. The number and size of segregation spots are increased by S-EMS, which contributes to the increase in the carbon macrosegregation of slabs. Figure 4b illustrates the relationship between the morphology of solidification and the ratio of segregation spot area (RSA) in the samples. The equiaxed crystal zone is enlarged by promoting the current intensity of S-EMS. However, the total segregation spaces and RSA are increased.

The morphology of dendrites is vital to control the distribution of the elements. As mentioned above, the denser dendrites were developed in the columnar crystal zone with the strong cooling rate during casting. Complete primary and secondary dendrites were observed in the equiaxed crystal zone of 0 A and 120 A slabs. The S-EMS reduces the temperature gradient<sup>26</sup> and increases the number of broken dendrites, and more nuclei were generated in the local space. The continuous growth behavior of columnar dendrites was transformed into stacking growth of the equiaxed dendrites by the S-EMS. The equiaxed dendrites without specific growth directions randomly accumulated at the solidification front, leading to more segregation spots being formed among the dendrites. To reduce the segregation of the grain-oriented silicon steel slabs in the present casting conditions, the equiaxed crystal zone should be minimized.

### Macrosegregation Behavior of Carbon

Figure 5 shows the degree of carbon segregation in the columnar zone is lower than that in the transition and equiaxed zone, indicating that carbon segregation tends to increase from the edge to the center of the slabs. Severe carbon segregation is controlled in the EZ of 0 A and 120 A slabs. Although the EZ is widened by S-EMS, severe carbon-positive and -negative segregation extends to the entire EZ. Figure 6 presents the statistical results that the degree of carbon segregation mainly

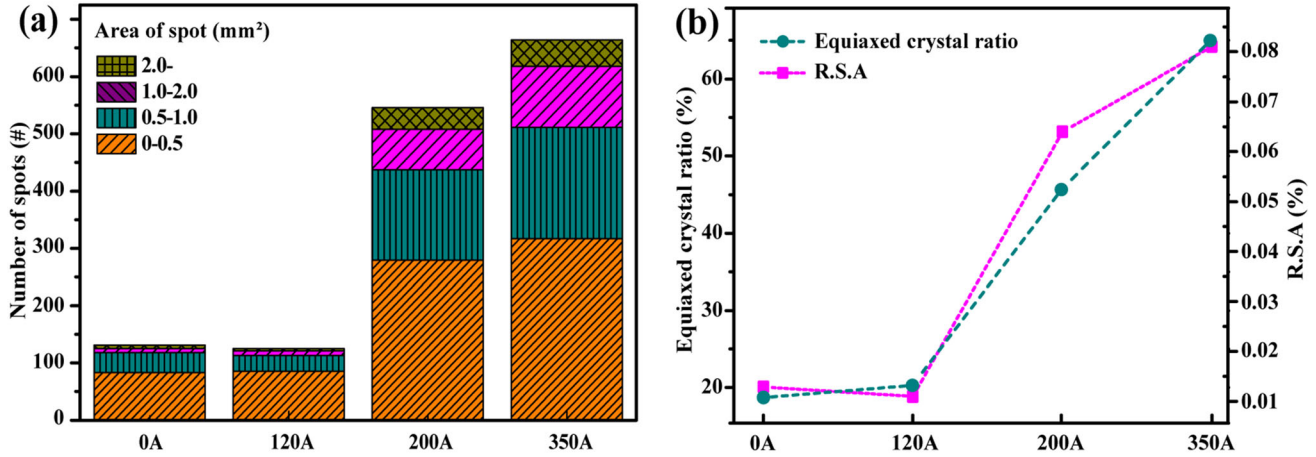


Fig. 4. Influence of S-EMS intensity on the spot: (a) the number and size of spots in slabs; (b) the ratio of segregation spots area and equiaxed crystal.

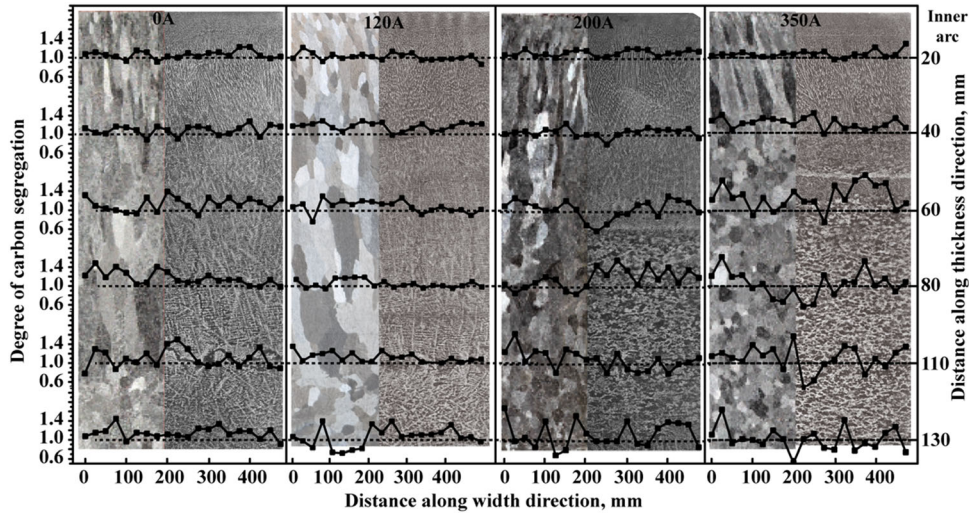


Fig. 5. Carbon distribution in the slab section.

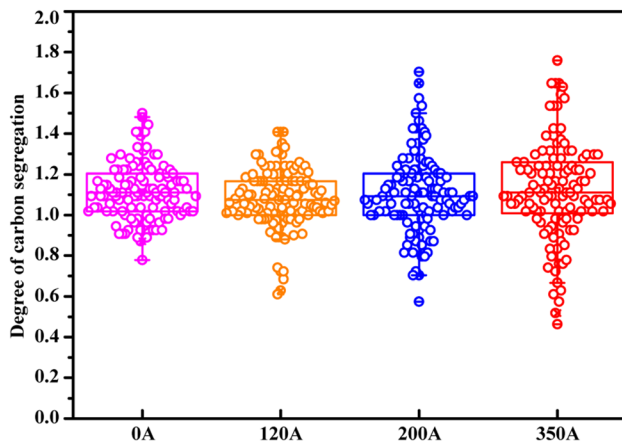


Fig. 6. Statistical results of carbon segregation.

ranges from 0.9 to 1.25, 0.9 to 1.25, 0.8 to 1.3, and 0.8 to 1.4 in the 0 A, 120 A, 200 A, and 350 A slabs, respectively. In previous studies, the segregation

behavior was easily attributed to the coarse columnar crystal structures<sup>8</sup> and the corresponding measures to decrease macrosegregation by soft reduction and electromagnetic stirring. However, segregation in the 0 A slab is similar to that in the 120 A slab and lower than that in the 200 A and 350 A slabs produced by soft reduction and S-EMS. Increasing the current intensities negatively affects the uniform distribution of carbon in grain-oriented silicon steel slabs.

In this study, the denser columnar crystals can more effectively reduce the carbon segregation of grain-oriented silicon steel. The variation in volume developed by solidification shrinkage and thermal contraction could be improved by squeezing the solidification shell during solidification. However, the effects of soft reduction on the columnar crystal and equiaxed crystal vary.<sup>13</sup> The columnar crystals are connected to the solidification shell, and the squeezing force directly acts on the mushy zone. Owing to the similar generation rate and direction,

the solidification section of the columnar crystals is regularly arranged. Thus, columnar crystals can more efficiently reduce segregation by soft reduction. The ratio of equiaxed crystals is significantly increased by S-EMS, and the effect of soft reduction on segregation is weakened. The macrosegregation is dominated by the density of dendrites rather than the type. In the present industrial production, denser dendrites were formed without or with slight intensity of S-EMS. However, experiments on controlling the cooling rate and increasing the total reduction should be carried out without S-EMS to further improve the solidification structures, defects, and carbon segregation.

### CONCLUSION

The solidification behavior of high-magnetic-induction grain-oriented silicon steel slabs was investigated in industrial S-EMS experiments. The current intensities were 0 A, 120 A, 200 A, and 350 A, and the frequency was 5 Hz. The results were as follows:

- (1) A wider equiaxed crystal zone and more symmetrical solidification structures were obtained by increasing the current intensities of S-EMS to 200 A and 350 A. The solidification structures of 0 A and 120 A slabs are dominated by cooling conditions, while the solidification structures of 200 A and 350 A slabs depend on the cooling conditions and the S-EMS stirring intensity.
- (2) The growth behavior of dendrites such as deflection and fracture is strongly influenced by the stirring intensity of S-EMS. Although the stirring intensity is strong enough, the central porosity cannot be eliminated in the present casting conditions.
- (3) The continuous growth behavior of columnar dendrites was transformed into stacking growth of equiaxed dendrites by the S-EMS, leading to the development of more segregation spots in the accumulation growth of equiaxed dendrites. The number, size, and ratio of segregation spots were significantly increased by the widened equiaxed crystal zone.
- (4) In the present industrial production, denser dendrites and uniform distribution of carbon were obtained in the slab without or with slight stirring intensity of S-EMS. To further improve the solidification structures and segregation behavior, controlling the cooling rate and increasing the total reduction were proposed without S-EMS.

### ACKNOWLEDGEMENTS

The authors are grateful for support from the National Science Foundation China (Grant No. 51574019), Open Project of State Key Laboratory of Advanced Special Steel, Shanghai University (SKLASS 2017-12), China, and Shougang Qian'an Iron and Steel Company.

### REFERENCES

1. M. Littman, *J. Magn. Magn. Mater.* 26, 1 (1982).
2. Z. Xia, Y. Kang, and Q. Wang, *J. Magn. Magn. Mater.* 23, 3229 (2008).
3. M.Q. Yan, H. Qian, P. Yan, H.J. Song, Y.Y. Shao, and W.M. Mao, *Acta Metall. Sin.* 48, 16 (2012).
4. Z. Liu, Z. Liu, J. Li, and Z. He, *Acta Metall. Sin.* 5, 33 (1992).
5. S. Choudhary, S. Ganguly, A. Sengupta, and V. Sharma, *J. Mater. Process. Tech* 243, 312 (2017).
6. Y. Tsuchida, I. Sugawara, S. Miyahara, T. Ishida, M. Ishikawa, and S. Matsumoto, *Trans. Iron. Steel. Int. Japan.* 22, B265 (1982).
7. M. Réger, B. Veró, Z. Csepeli, and Á. Szélig, *Mater. Sci. Forum* 508, 233 (2006).
8. H. Zhang, E. Wang, and G. Jia, *J. He. Acta. Metall. Sin.* 14, 227 (2001).
9. H.T. Liu, Z.Y. Liu, G.M. Cao, C.G. Li, and G.D. Wang, *J. Magn. Magn. Mater.* 323, 2648 (2011).
10. T. Itakura, T. Ishige, M. Nakada, H. Nakashima, and M. Tada, *Steelmak. Confer.* 77, 291 (1994).
11. F. Satou, H. Esaka, and K. Shinozuka, *Tetsu. To. Hagane. J. Iron. Steel. Ins. Japan.* 99, 108 (2013).
12. Y. Tsuchida, M. Nakada, U. Sugawara, S. Miyahara, K. Murakami, and S. Tokushige, *Trans. Iron. Steel. Int. Japan.* 24, 899 (1984).
13. Z. Xu, X. Wang, F. Huang, L. Zhou, W. Wang, and Y. Yin, *J. U. Sci. Technol. Beijing.* 36, 751 (2014).
14. H. Wu, N. Wei, Y. Bao, G. Wang, and C. Xiao, *J. Liu. Int. J. Min. Met. Mater.* 18, 159 (2011).
15. H. An, Y. Bao, M. Wang, and L. Zhao, *Metal. Res. Technol.* 114, 405 (2017).
16. H. Sun, L. Li, J. Wang, X. Cheng, and F. Zhou, *Ironmak. Steelmak.* 45, 708 (2017).
17. B. Lu, F. Qi, and W. Shen, *J. Liu. Spec. Steel.* 38, 40 (2017).
18. E. Wang, E. Jiang, G. Zhan, and A. Deng, *J. He. Mater. Sci. Forum.* 706–709, 2480 (2012).
19. Y. Yu and B. Li, *Acta Metall. Sin.* 42, 540 (2006).
20. K. Spitzer, *Prog. Cryst. Growth Charact. Mater.* 38, 59 (1999).
21. J. Pilling and A. Hellawell, *Metall. Mater. Trans.* 27A, 229 (1996).
22. T. Cool and P. Voorhees, *Acta Mater.* 127, 359 (2017).
23. X. Wang, S. Wang, L. Zhang, S. Sridhar, A. Conejo, and X. Liu, *Metall. Mater. Trans. A* 47, 5496 (2016).
24. L. Lu, K. Nogita, S. McDonald, and A. Dahle, *JOM* 56, 52 (2004).
25. T. Brune, K. Kortzak, D. Senk, N. Reuther, and M. Schäperkötter, *Steel Res. Int.* 86, 33 (2015).
26. S. Kunstreich, *Metal. Res. Technol.* 100, 1043 (2003).

**Publisher's Note** Springer Nature remains neutral with regard to jurisdictional claims in published maps and institutional affiliations.